Chemical trends of stability and band alignment of lattice-matched II-VI/III-V semiconductor interfaces

Hui-Xiong Deng,[1,*] Jun-Wei Luo,[1] and Su-Huai Wei[2,†]

[1]*State Key Laboratory for Superlattices and Microstructures, Institute of Semiconductors, Chinese Academy of Sciences, Post Office Box 912, Beijing 100083, China*

[2]*National Renewable Energy Laboratory, Golden, Colorado 80401, USA*

(Received 10 December 2014; revised manuscript received 4 February 2015; published 26 February 2015)

Using the first-principles density functional theory method, we systematically investigate the structural and electronic properties of heterovalent interfaces of the lattice-matched II-VI/III-V semiconductors, i.e., ZnTe/GaSb, ZnSe/GaAs, ZnS/GaP, and ZnO/GaN. We find that, independent of the orientations, the heterovalent superlattices with period $n = 6$ are energetically more favorable to form nonpolar interfaces. For the [001] interface, the stable nonpolar interfaces are formed by mixing 50% group-III with 50% group-II atoms or by mixing 50% group-V with 50% group-VI atoms; for the [111] nonpolar interfaces, the mixings are 25% group-III (II) and 75% group-II (III) atoms or 25% group-V (VI) and 75% group-VI (V) atoms. For all the nonpolar interfaces, the [110] interface has the lowest interfacial energy because it has the minimum number of II-V or III-VI "wrong bonds" per unit interfacial area. The interfacial energy increases when the atomic number of the elements decreases, except for the ZnO/GaN system. The band alignments between the II-VI and III-V compounds are drastically different depending on whether they have mixed-cation or mixed-anion interfaces, but the averaged values are nearly independent of the orientations. Similarly, other than ZnO/GaN, the valence-band offsets also increase as the atomic number of the elements decreases. The abnormal trends in interfacial energy and band alignment for ZnO/GaN are primarily attributed to the very short bond lengths in this system. The underlying physics behind these trends are explained.

DOI: 10.1103/PhysRevB.91.075315 PACS number(s): 73.21.Cd, 79.60.Jv, 72.80.Ey, 71.15.Nc

I. INTRODUCTION

It has been proposed that mixing lattice-match II-VI and III-V semiconductors could be an efficient way to tune the material properties for specific applications [1–7] because the II-VI and III-V usually have much larger tunability than isovalent semiconductor alloys [e.g., the band gap of GaAs (1.5 eV) is much smaller than that of ZnSe (2.8 eV), even though they are lattice matched; see Table I]. For example, lattice-matched ZnO/GaN alloys have been suggested as good candidates for electrodes for high-efficiency solar hydrogen production through photoelectrochemical water splitting [3,9,10]; lattice-matched ZnSe/GaAs and ZnTe/GaSb heterojunctions are proposed to be high-quality blue-green emitters [11,12]. ZnTe/GaSb have also been proposed as good candidates for tandem solar cell absorber materials because GaSb has a band gap of 0.8 eV and ZnTe has a band gap of 2.4 eV; therefore, their alloys and superlattices can cover a large range of the solar spectrum without significant change in the lattice constant [7]. However, despite the lattice match between the II-VI and III-V compounds, mixing the pair of II-VI and III-V to form a disordered alloy is usually difficult because for heterovalent (II-VI or III-V) alloys there will inevitably be many wrong II-V and III-VI bonds which will significantly increase the alloy formation energy [6]. To reduce the number of wrong bonds in the system, one effective way could be forming superlattices instead of disordered alloys because for a superlattice the II-V (with a deficiency of 1/4 of an electron) and III-VI (with 1/4 excess electrons) wrong bonds will only occur at the interface. However, it is not clear what kind of interfacial structures are more stable for the superlattices with different orientation and how the interface atomic structures affect the material properties such as the band offset [13–22]. It is also not clear how these material properties change with atomic numbers, for example, from ZnTe/GaSb to ZnSe/GaAs to ZnS/GaP to ZnO/GaN.

In this paper, we select the lattice-matched heterovalent Zn-VI/Ga-V (VI = Te, Se, S, O; V = Sb, As, P, N) semiconductor superlattices as examples, and analyze their structural stability and electronic properties of the interfaces with different orientations and interfacial atomic configurations. Within the *ab initio* total-energy and electronic structure calculations, we find that for all the orientations ([100], [110], [111], etc.) the heterovalent superlattices with period $n = 6$ are energetically more favorable to form nonpolar interfaces. For all the different orientations, the [110] nonpolar interface has the lowest interfacial energy, because the [110] nonpolar interface has the least number of wrong bonds per unit interfacial area. The calculated band offsets also show that although the valence-band offsets (VBOs) for the nonpolar mixed-cation and mixed-anion interfaces are very different the average offset is nearly orientation independent. The interfacial formation energy and valence-band offset increases when the atomic number decreases, but for the ZnO/GaN pair the trend reverses due to the very short bond length of the ZnO/GaN systems.

II. METHODS OF CALCULATIONS

In this study, the model $(\text{II-VI})_6/(\text{III-V})_6$ zinc-blende superlattice structures along [001], [110], and [111] directions (Fig. 1, left side), respectively, are investigated. For the

*hxdeng@semi.ac.cn
†swei@nrel.gov

TABLE I. Summary of the experimental lattice constants and band gaps of ZnTe/GaSb, ZnSe/GaAs, ZnS/GaP, and ZnO/GaN compounds in pairs. All data come from Ref. [8].

Pairs	Lattice constant (Å)	Band gap (eV)
ZnTe/GaSb	6.088/6.095	2.394/0.822
ZnSe/GaAs	5.667/5.653	2.822/1.519
ZnS/GaP	5.405/5.450	3.723/2.350
ZnO/GaN		
a	3.249/3.190	3.441/3.503
c	5.204/5.189	

atomic arrangements parallel to the interface, we choose the $(\sqrt{2}\times\sqrt{2})$,(1×1), and (2×2) supercells, respectively, for [001], [110], and [111] superlattices (Fig. 1, right side), in which a_1 and a_2 are the basis vectors of lateral planes. Actually, because we only consider the atomic configurations within a few atomic layers near the interface, the total number of nonequivalent interfacial structures is not quite large. Therefore, we just enumerate all the possible nonequivalent interfacial structures to search for the interfacial ground state along different orientations. The total energies are calculated using the density functional theory [23,24] within generalized-gradient approximations (GGAs) [25], as implemented in the Vienna *ab initio* simulation package (VASP) [26–28]. The electron and core interactions are included based on the frozen-core projected-augmented-wave approach [29]. The cutoff energy for the wave-function expansion is 450 eV. For the [001] and [110] superlattices, a k-point grid density [30] of $8\times 8\times 1$ was employed in the first Brillouin zone, and for the [111] superlattice a $6\times 6\times 1$ k-point grid was used. In the relaxation process, all the atoms are allowed to relax until the quantum-mechanical forces acting on them become less than 0.02 eV/Å.

The interfacial energy is defined:

$$E_{\rm int}=\frac{E_{\rm tot}[(AX)_n(BY)_n]-[nE_{\rm tot}(AX)+nE_{\rm tot}(BY)]}{2S}, \quad (1)$$

where $E_{\rm tot}[({\rm AX})_n\,({\rm BY})_n]$, $E_{\rm tot}({\rm AX})$, and $E_{\rm tot}({\rm BY})$ are the total energies of the superlattice, bulk AX, and BY, respectively. S represents the interfacial area. Convergence of the interfacial energy with respect to the slab thickness n is checked. Convergence tests show that $n=6$ is sufficient [20] to converge the interfacial energy to within 0.1 meV/Å^2.

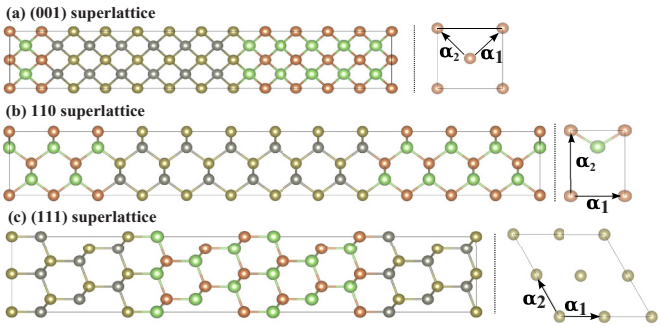

FIG. 1. (Color online) Schematic plots of (a) [100], (b) [110], and (c) [111] $(\text{II-VI})_6/(\text{III-V})_6$ superlattices. The right side of the plot shows the lateral atomic arrangements parallel to the interface. $\boldsymbol{a_1}$ and $\boldsymbol{a_2}$ are the basis vectors of the lateral plane. The green, orange, gray, and dark yellow balls indicate the group-III, -V, -II, and -VI atoms, respectively. The color scheme is the same for all figures in the paper.

III. RESULTS AND DISCUSSIONS

A. [001] orientation

Figure 2 shows the interfacial energies of $(\text{GaSb})_6\,(\text{ZnTe})_6$ (a) [001], [b] [110], and (c) [111] superlattices calculated for all nonequivalent interfacial atomic configurations. We see from Fig. 2(a) that the structures A, B, C, and D have nearly the same minimum energy of around 6.6 meV/Å^2 for the [001] growth orientations. The corresponding atomic configurations are presented in Fig. 3. We found that the structures A and B are the mixed-cation interfaces, and C and D are the mixed-anion interfaces. As a comparison, we also list the abrupt interface, which has interfacial energy of 19.13 meV/Å^2, much higher than the low-energy interfacial structures (A, B, C, and D). It is clear that in the case of [001] $\sqrt{2}\times\sqrt{2}$ superlattices each atomic layer has two atoms and at least four "wrong bonds" (i.e., Ga-Te or Zn-Sb bonds) at the interface. In the structures A, B, C, and D, the mixed interfaces are formed either by one Ga atom plus one Zn atom or by one Sb atom plus one Te atom. In other words, the stable mixed interfaces are constructed by 50% Sb and 50% Te atoms or by 50% Ga and 50% Zn atoms, as

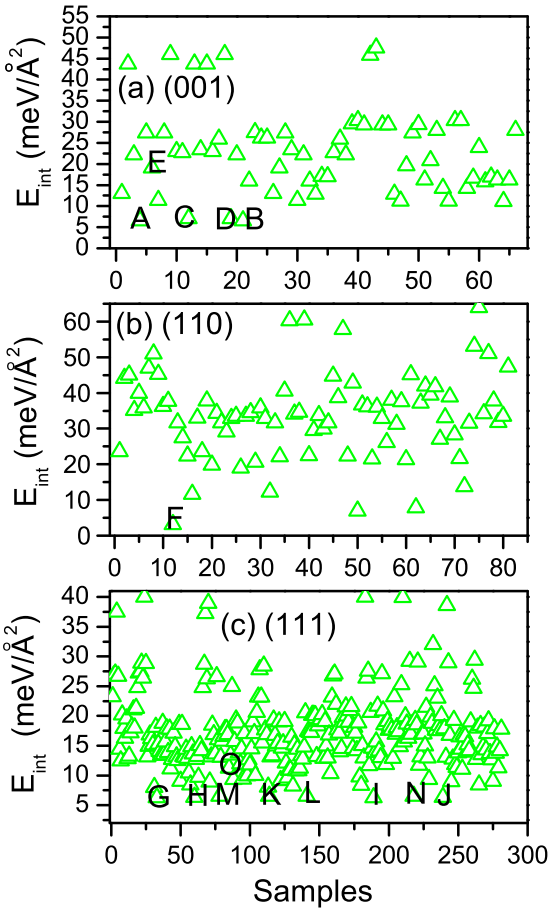

FIG. 2. (Color online) Interfacial energies (meV/Å^2) of ZnTe/GaSb (a) [001], (b) [110], and (c) [111] interfaces calculated for all nonequivalent interfacial atomic configurations.

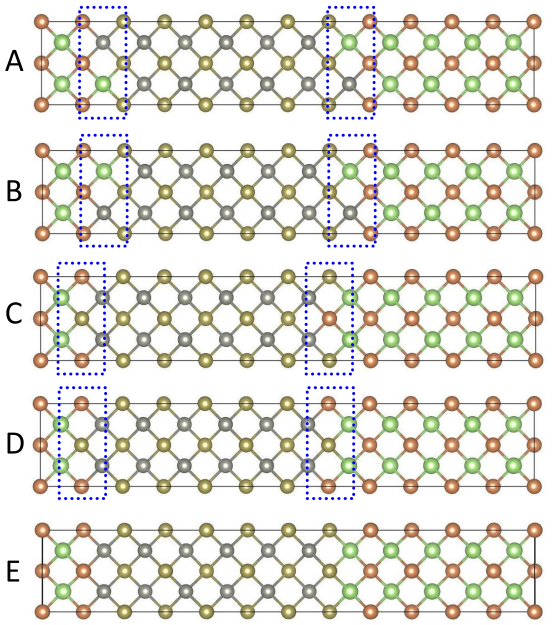

FIG. 3. (Color online) Atomic configurations of (GaSb)/(ZnTe) [001] interfaces corresponding to A, B, C, D, and E points in Fig. 2(a). Structures A and B are the mixed-cation interfaces, C and D are the mixed-anion interfaces, and E is for a sharp interface.

predicted by previous studies [20–22], and there are two Ga-Te and two Zn-Sb wrong bonds at the interfaces. As we know, the Zn-Sb bond is an acceptor bond, providing 1/4 holes, and the Ge-Te bond is a donor bond, providing 1/4 electrons. Thus, at the 50:50 mixed interfaces the equal acceptor and donor bonds will be fully and locally compensated, and thus no excess holes or electrons are accumulated near the interfaces. On the other hand, because it has only one kind of wrong bonds, the Ga-Te or Zn-Sb bond, the abrupt interface E will accumulate electrons at the Ga-Te interface or holes at the Zn-Sb interface. Consequently there will exist an electric field in this type of superlattices. To verify the above analysis, we plot the local potential distributions of structures A, B, C, D, and E along the [001] orientation, as shown in Fig. 4. It is clearly seen that in the structures A, B, C, and D there is no electric field through the superlattices, and thus they are nonpolar, whereas in structure E with the abrupt interface there apparently exists an electric field through the superlattice, and it is thus polarized. Figure 5 shows the total density of states (DOS) of structures A, B, C, D, and E of (GaSb)/(ZnTe) [001] superlattices. It is clearly shown that the structures A, B, C, and D have a band gap based on GGA calculations, while structure E does not. Although the GGA calculations underestimate the band gap by about 30–50% [31] in this system, the relative values of the band gap in these structures are physically meaningful. That is to say, the band gaps of structures A, B, C, and D are always larger than that of structure E. This is consistent with the general expectation that the large band-gap materials are in general more stable than the smaller band-gap materials.

B. [110] orientation

Figure 2(b) shows the interfacial energies of $(GaSb)_6$ $(ZnTe)_6$ [110] superlattices for different nonequivalent interfacial atomic structures. We find that the stablest interfacial structure F has the interfacial energy of 3.15 meV/Å^2, which is lower than that in the [001] interface. The

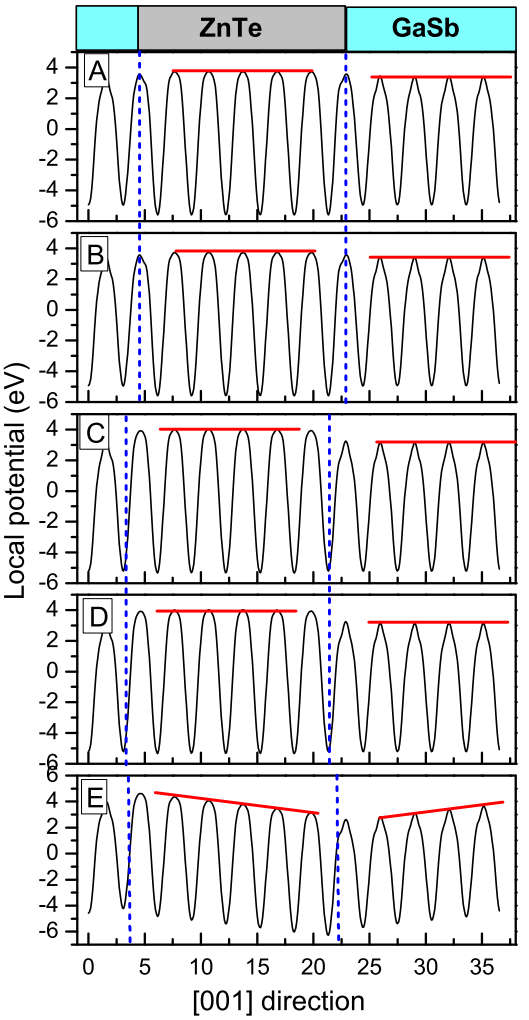

FIG. 4. (Color online) Corresponding potential distributions of interfacial structures A, B, C, D, and E along growth orientation for the (GaSb)/(ZnTe) [001] $\sqrt{2} \times \sqrt{2}$ superlattices. The red lines indicate the top of the potential along the growth direction of the superlattice and show schematically whether or not there is an electric field through the superlattice. This scheme is the same for Figs. 6 and 8 in this paper.

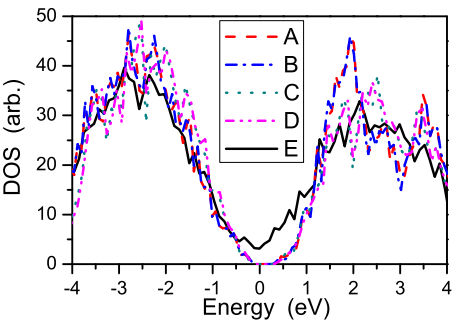

FIG. 5. (Color online) Total density of states (DOS) of structures A, B, C, D, and E for the (GaSb)/(ZnTe) [001] superlattices. The Fermi level is set to be 0 eV.

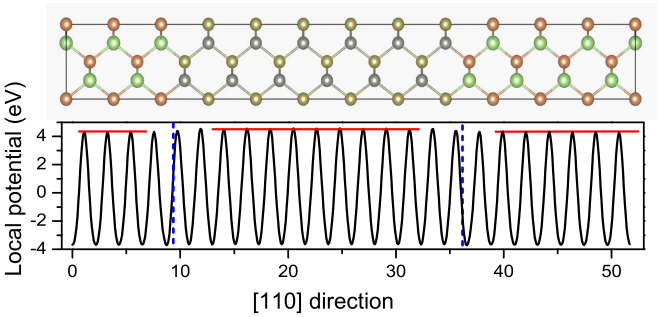

FIG. 6. (Color online) Atomic configuration (the upper panel) and potential distribution (the bottom panel) of structure F of the ZnTe/GaSb [110] 1×1 superlattice.

corresponding atomic structure and local potential of structure F are presented in Fig. 6. We find that the interfaces of structure F are abrupt. The plot of local Coulomb potential shows that there is no electric field through the superlattice, which is consistent with the fact that the interface is nonpolar because the (1×1) [110] interface has exactly one Ga-Te and one Zn-Sb wrong bond, which can fully compensate each other, so that no excess charges are accumulated near the interfaces.

C. [111] orientation

Figure 2(c) shows the interfacial energies of $(GaSb)_6(ZnTe)_6$ [111] superlattices for different nonequivalent interfacial atomic structures. We find that the structures G, H, I, J, K, L, M, and N have nearly the same lowest interfacial energy of around 6.3 meV/Å^2. The corresponding atomic configurations are presented in Fig. 7. Apparently the structures G, H, I, and J have the mixed-cation interfaces, while K, L, M, and N have the mixed-anion interfaces. As a comparison, we also list the structure O with the abrupt interfaces, which has an interfacial energy of 8.91 meV/Å^2, larger than that of mixed interfaces. Figure 8 presents the corresponding local potential of structures G–O along the [111] orientation. It is clear that for the mixed interfaces there is no electric field at the center of the superlattice. Therefore, we call these interfaces nonpolar although the two interfaces are not exactly the same. For the abrupt structure O there apparently exists an electric field through the superlattice, which is polarized. It is also interesting to see from Fig. 7 that the stable mixed interfaces for the [111] 2×2 superlattices are constructed by one Ga (Zn) and three Zn (Ga) atoms (structures G, H, I, and J) or by one Sb (Te) and three Te (Sb) atoms (structures K, L, M, and N), i.e. a 25–75% mixture, which is distinct from the case of [001]-oriented superlattices, in which the stable mixed interfaces are formed with a 50:50 mixture of Ga and Zn or Sb and Te atoms. More generally, in the case of ZB [111] superlattices, if the lateral dimension of the unit cell is $N_1 \times N_2$ (N_1 and N_2 are integers), then each atomic layer has $N = N_1 \times N_2$ atoms [Fig. 1(c)], and so the minimum of wrong bonds of the abrupt interface is N, which are parallel to [111] directions. Thus when M II (III) atoms are changed to III (II) atoms to form mixed-cation interfaces, or M VI (V) atoms are changed to V (VI) atoms to form mixed-anion interfaces, it will eliminate M wrong bonds

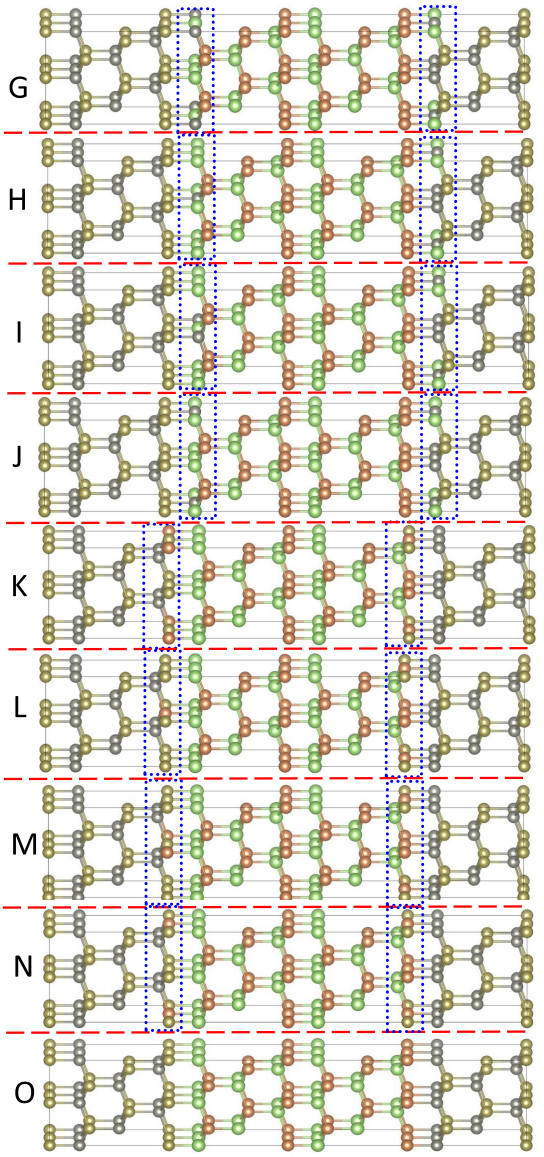

FIG. 7. (Color online) Atomic structures of ZnTe/GaSb [111] 2×2 interfaces corresponding to G, H, I, J, K, L, M, N, and O sites in Fig. 2(c). Structures G, H, I, and J are the mixed-cation interfaces with different symmetries, and K, L, M, and N are the mixed-anion interfaces with different symmetries. As a comparison, we also list the abrupt interface (structure O).

parallel to the [111] direction and simultaneously give rise to $3M$ wrong bonds in the other three directions. The new generated and non-[111]-direction $3M$ wrong bonds have the opposite bond characters (acceptor or donor type) compared to that of the remaining $N - M$ wrong bonds parallel to the [111] direction near the interface. Consequently, in order to keep local charge neutrality and form nonpolar interfaces, it should satisfy the relation $N - M = 3M$. That is why, for the mixed nonpolar interfaces, the ratio of the number of atoms is $M/(N - M) = 1/3$, i.e., a 25:75 mixture.

D. Comparison between [001], [110], and [111] orientations

In the previous sections, we studied the stability of [001], [110], and [111] ZnTe/GaSb superlattices and found that the

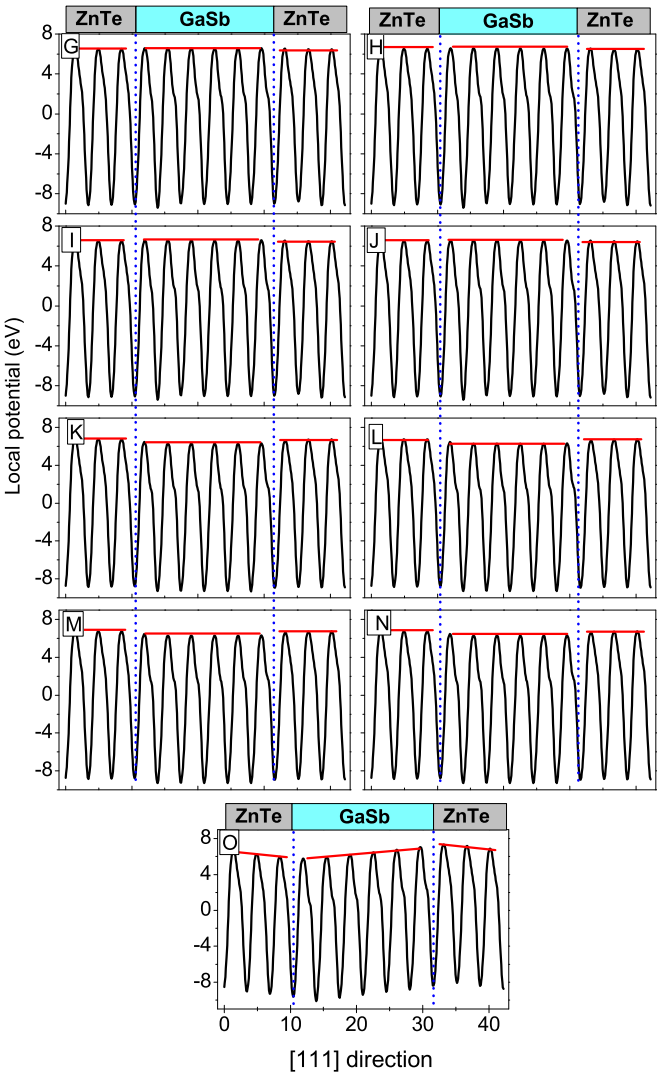

FIG. 8. (Color online) Potential distributions for the mixed-cation interfaces [i.e., G, H, I, and J in Fig. 2(c)] and mixed-anion interfaces [K, L, M, and N in Fig. 2(c)], respectively, along the [111] direction for the (GaSb)/(ZnTe) [111] 2×2 superlattices. As a comparison, we also show the potential distributions for the pure interface (structure O).

energetically stable structures all have nonpolar interfaces. However, these stable nonpolar interfaces along different orientations have very different atomic compositions. For example, the stable nonpolar interfaces along [001] orientation are mixed by 50% group-III and 50% group-II atoms or by 50% group-V and 50% group-VI atoms, and for the [111] orientation the stable nonpolar interfaces are mixed by 25% group-III (II) and 75% group-II (III) atoms or by 25% group-V (VI) and 75% group-VI (V) atoms, whereas the [110] nonpolar interfaces are fully abrupt. The reason why the nonpolar interfaces have the lowest interfacial energy in all these growth orientations is mainly due to the fact that it has the lowest Coulomb energy near the interface. Figure 9 shows the schematic Coulomb interactions of the ZnTe/GaSb superlattice in forming the [001] polar and nonpolar interfaces. Apparently, at the polar interface there are excess holes at the Zn-Sb interface and electrons at the

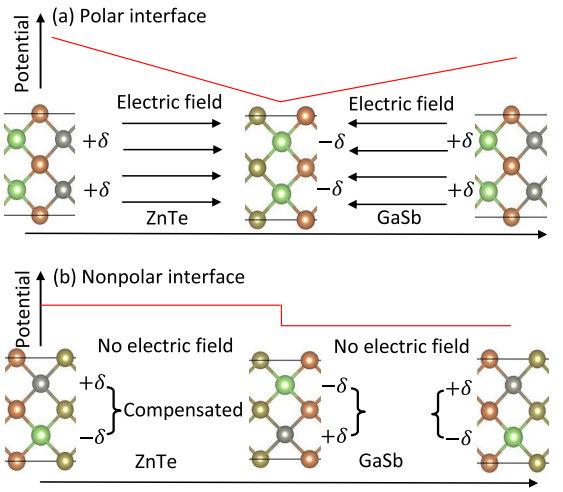

FIG. 9. (Color online) Schematic Coulomb interactions of ZnTe/GaSb [001] superlattice systems in forming (a) polar and (b) nonpolar interfaces.

Ga-Te interface. When these two interfaces are far enough apart, the Coulomb interaction between these two interfaces is reduced. However, the Coulomb interaction at each interface increases the interfacial energy due to the presence of hole-hole or electron-electron Coulomb repulsion [Fig. 9(a)]. However, for the nonpolar interface, because it has equal acceptor and donor bonds on a single interface, the excess holes can be fully and locally compensated by the electrons at the each interface layer. Therefore the Coulomb interaction derived from excess holes or electrons becomes attractive. As a result, the nonpolar interfaces have low interface energy [Fig. 9(b)].

E. Chemical trends for various lattice-matched (III-V)/(II-VI) superlattices

Table II lists the interfacial energies of nonpolar interfaces along different orientations for the lattice-matched ZnTe/GaSb, ZnSe/GaAs, ZnS/GaP, and ZnO/GaN heterostructures. We find the interfacial energy of stable interface structures along different orientations has $E_{\rm int}^{001} > E_{\rm int}^{111} > E_{\rm int}^{110}$ in all these systems. As in our previous discussions, the number of wrong bonds per unit area at the interfacial region for various orientations is also important in determining the interfacial energy of nonpolar interfaces. The more wrong bonds per unit interfacial area, the larger the interfacial energy is. The

TABLE II. Calculated interfacial energies $E_{\rm int}$ (in meV/Å^2) of the II-VI/III-V superlattices along [001], [110], and [111] orientations. The last row shows the number of wrong bonds per unit interfacial area. Here a is the lattice constant.

System	[001]	[110]	[111]
ZnTe/GaSb	6.61	3.15	6.29
ZnSe/GaAs	7.99	3.62	7.05
ZnS/GaP	9.24	3.60	8.31
ZnO/GaN	8.02	2.88	4.83
Number of wrong bonds per unit area	$4/a^2$	$4/\sqrt{2}a^2$	$6/\sqrt{3}a^2$

interfacial area for [001], [110], and [111] superlattices is a^2, $\frac{\sqrt{2}}{2}a^2$, and $\sqrt{3}a^2$, respectively (Fig. 1). Here a is the lattice constant. The corresponding minima of wrong bonds of the nonpolar interface are 4, 2, and 6. Hence, the minima of wrong bonds per unit interfacial area are $4/a^2$, $4/\sqrt{2}a^2$, and $6/\sqrt{3}a^2$ for the [001], [110], and [111] nonpolar interfaces, respectively. Apparently, $4/a^2 > 6/\sqrt{3}a^2 > 4/\sqrt{2}a^2$. That is the reason why for the nonpolar interfaces $E_{\rm int}^{001} > E_{\rm int}^{111} > E_{\rm int}^{110}$. Because the bond strength (bulk modulus) and the number of wrong bonds per area increase as the atomic number decreases, the interfacial energy generally increases as the atomic number of the compounds decreases. However, for ZnO/GaN, due to the very short bond length, the Coulomb interaction between the atoms and layers lowered its interfacial formation energies.

F. Arbitrary orientation

To calculate the interfacial energy along arbitrary growth orientation, we expand the interfacial energy for orientation (l,m,n) or angle (θ,ϕ) in terms of the cubic lattice harmonics with $l_{\rm max} = 6$ [32,33]:

$$E_{\rm int}(\theta,\phi) = a + bK_4(\theta,\phi) + cK_6(\theta,\phi), \tag{2}$$

where

$$\begin{aligned} K_4(\theta,\phi) &= \sin(\theta)^4\cos(\phi)^4 + \sin(\theta)^4\sin(\phi)^4 + \cos(\theta)^4 - \tfrac{3}{5}, \\ K_6(\theta,\phi) &= \sin(\theta)^4\cos(\theta)^2\cos(\phi)^2\sin(\phi)^2 \\ &\quad + \tfrac{1}{22}\big[\sin(\theta)^4\cos(\phi)^4 + \sin(\theta)^4\sin(\phi)^4 \\ &\quad + \cos(\theta)^4 - \tfrac{3}{5}\big] - \tfrac{1}{105}, \end{aligned} \tag{3}$$

where $\theta \in [0,\pi]$ and $\phi \in [0,2\pi)$. The parameters a, b, and c can be fitted using the interfacial energies of [001] ($\theta = 0$), [110] ($\theta = \pi/2, \phi = \pi/4$), and [111] ($\theta = \arccos(1/\sqrt{3}), \phi = \pi/4$) directions. In order to identify the lowest interfacial energy orientation $(\theta_{\rm min}, \phi_{\rm min})$ according to Eq. (2), we need to solve the following equations:

$$\begin{aligned} \frac{\partial E_{\rm int}(\theta,\phi)}{\partial\theta} &= 0 \\ \frac{\partial E_{\rm int}(\theta,\phi)}{\partial\phi} &= 0. \end{aligned} \tag{4}$$

Using our calculated values, we find the minimum interfacial energy occurs at (θ, ϕ) equal to $(\frac{\pi}{4}, 0)$, $(\frac{\pi}{4}, \frac{\pi}{2})$, $(\frac{\pi}{4}, \pi)$, $(\frac{\pi}{4}, \frac{3\pi}{2})$, $(\frac{\pi}{2}, \frac{\pi}{4})$, $(\frac{\pi}{2}, \frac{3\pi}{4})$, $(\frac{\pi}{2}, \frac{5\pi}{4})$, $(\frac{\pi}{2}, \frac{7\pi}{4})$, $(\frac{3\pi}{4}, 0)$,$(\frac{3\pi}{4}, \frac{\pi}{2})$, $(\frac{3\pi}{4}, \pi)$, $(\frac{3\pi}{4}, \frac{3\pi}{2})$, which all are equivalent to the [110] direction. This result further confirmed that for thick superlattices the [110] nonpolar interface has the lowest interfacial energy among all growth orientations.

G. Band offsets

Another essential quantity in any interface is the band offset, and for the heterovalent interface it depends sensitively on the orientations and atomic configurations near the interfaces. Theoretical simulations of the band offset are basically following the procedure used in photoemission core level spectroscopy, in which the VBOs of two compounds are obtained by [13,34,35] $\Delta E_v(AX/BY) = \Delta E_{v,C'}(BY) - \Delta E_{v,C}(AX) + \Delta E_{C',C}(AX/BY)$, where $\Delta E_{v,C}(AX) = E_v(AX) - E_C(AX)$ [the same for $\Delta E_{v,C'}(BY)$] is the energy difference between the core level and valence-band maximum for the pure AX compound, and $\Delta E_{C',C}(AX/BY) = E_{C'}(BY) - E_C(AX)$ is the core level energy difference between AX and BY at the AX/BY heterostructure. Table III shows the calculated VBOs of nonpolar interfaces for ZnTe/GaSb, ZnSe/GaAs, ZnS/GaP, and ZnO/GaN heterostructures along different growth orientations, and comparison with the corresponding experimental results when possible. In the [001] orientation, the mixed-cation A and mixed-anion C structures are chosen, and in the [111] orientation the mixed-cation G and mixed-anion K are chosen for the VBO calculations. It is interesting to see that although the VBOs for the nonpolar mixed-cation structures are always larger than that for the nonpolar mixed-anion structures in the [001] or [111] orientation the average of the band offsets is nearly equal to that of intrinsic nonpolar [110] orientation. Except for ZnO/GaN, the VBOs increase monotonically from ZnTe/GaSb to ZnSe/GaAs to ZnS/GaP, which is consistent with the fact that the VBM consists mainly of anion p orbitals and the difference of atomic chemical potential of p orbits of group-V and group-VI atoms increases from $5p$ (Sb-Te) to $4p$ (As-Se) to $3p$ (P-S) [40]. For ZnO/GaN, the trend is reversed again because for this system with small bond lengths the level repulsion between anion p and cation d states is much

TABLE III. Valence-band offsets (in eV) of nonpolar interfaces for the nonisovalent II-VI/III-V semiconductors along [001], [110], and [111] directions, respectively. A positive number indicates that the III-V has a higher VBM than the II-VI compound.

	[001] orientation			[110] orientation	[111] orientation			
Systems	Mixed cation	Mixed anion	Average	Abrupt	Mixed cation	Mixed anion	Average	Expt.
ZnTe/GaSb	0.89	0.37	0.63	0.63	0.91	0.40	0.65	0.60[a], 0.79 [b]
ZnSe/GaAs	1.03	0.39	0.71	0.72	1.05	0.40	0.72	0.93[c], 1.10 [d]
ZnS/GaP	1.20	0.45	0.82	0.86	1.22	0.47	0.85	
ZnO/GaN	0.87	−0.02	0.43	0.38	0.82	−0.12	0.35	0.7–1.0[e],[f]

[a]From Ref. [36].
[b]From Ref. [37].
[c]From Ref. [38].
[d]From Ref. [39].
[e]From Ref. [14].
[f]From Ref. [16].

larger for ZnO than GaN because Zn has much shallower 3*d* orbitals than Ga 3*d* orbitals, thus reducing the band offsets. The increased $p-p$ repulsion between anion and cation p orbitals is also partially responsible for the reduced band offset. It is also interesting to notice that, although all the nonpolar interfaces of [001] or [111] orientation have nearly the same interfacial energies, the VBOs of these nonpolar interfaces in the same orientation could have large difference due to the difference of atomic configurations near the interfaces. It should be noted that, compared to the hybrid functional (HSE) [41] or quasiparticle GW method [42,43], although the PBE underestimates the band gaps, the error on the band offsets is largely canceled because we are calculating the energy difference between compounds in the same row [44]. However, for ZnO/GaN, the large overestimation of *p-d* coupling in ZnO could underestimate the calculated VBO for this system.

IV. CONCLUSIONS

In summary, based on first-principle calculations, we investigated structural stability and band alignment of lattice-matched II-VI/III-V semiconductor interfaces, i.e., ZnTe/GaSb, ZnSe/GaAs, ZnS/GaP, and ZnO/GaN along different growth orientations. We found that the abrupt [001] and [111] interfaces are polar interfaces, whereas the abrupt [110] interface is nonpolar. These [001] and [111] polar interfaces are highly unstable and will reconstruct into a chemically mixed geometry so as to remove the polarity and reduce the Coulomb repulsion energy near the interfaces. For the case of [001] interfaces, the stable nonpolar interfaces are mixed with 50% group-III and 50% group-II atoms or with 50% group-V and 50% group-VI atoms. While in the [111] orientation, the stable nonpolar interfaces are formed by mixing 25% group-III (II) and 75% group-II (III) atoms or by 25% group-V (VI) and 75% group-VI (V) atoms. Among all the nonpolar interfaces, the [110] nonpolar interface is found to have the lowest interfacial energy because it has the minimum number of II-V or III-VI wrong bonds at the interface per unit interfacial area. The interfacial energy increases when the atomic number of the elements decreases except for ZnO/GaN, which has a lower interfacial formation energy than the ZnS/GaP system due to the very short bond lengths in ZnO/GaN. The band alignments between the II-VI and III-V compounds are drastically different whether they have mixed-cation or mixed-anion interfaces, but the averaged values are nearly independent of the orientations. The valence-band offsets increase as the atomic number of the elements decreases, except for ZnO/GaN, which has a smaller VBM offset than ZnS/GaP because of the short bond lengths and large $p-d$ repulsion in ZnO/GaN system. These general trends are expected to hold in other related systems.

ACKNOWLEDGMENTS

The work at Institute of Semiconductors, Chinese Academy of Sciences was supported by the National Basic Research Program of China (973 Program) Grant No. G2009CB929300 and the National Natural Science Foundation of China under Grants No. 61121491, No. 11474273, and No. 11104264. The work at National Renewable Energy Laboratory was supported by the US Department of Energy under Contract No. DE-AC36-08GO28308.

[1] W. R. L. Lambrecht and B. Segall, Phys. Rev. B **41**, 2832 (1990).
[2] R. Nicolini, L. Vanzetti, G. Mula, G. Bratina, L. Sorba, A. Franciosi, M. Peressi, S. Baroni, R. Resta, A. Baldereschi, J. E. Angelo, and W. W. Gerberich, Phys. Rev. Lett. **72**, 294 (1994).
[3] K. Maeda, T. Takata, M. Hara, N. Saito, Y. Inoue, H. Kobayashi, and K. Domen, J. Am. Chem. Soc. **127**, 8286 (2005).
[4] A. Colli, E. Pelucchi, and A. Franciosi, Appl. Phys. Lett. **83**, 81 (2003).
[5] A. Frey, U. Bass, S. Mahapatra, C. Schumacher, J. Geurts, and K. Brunner, Phys. Rev. B **82**, 195318 (2010).
[6] S. Wang and L.-W. Wang, Phys. Rev. B **83**, 115208 (2011).
[7] H.-X. Deng, B. Huang, and S.-H. Wei, Comput. Mater. Sci. **98**, 340 (2015).
[8] O. Madelung, *Semiconductors: Data Handbook* (Springer, Berlin, 2004).
[9] K. Maeda, K. Teramura, D. Lu, T. Takata, N. Saito, Y. Inoue, and K. Domen, Nature (London) **440**, 295 (2006).
[10] S. Wang and L.-W. Wang, Phys. Rev. Lett. **104**, 065501 (2010).
[11] M. A. Haase, J. Qiu, J. M. DePuydt, and H. Cheng, Appl. Phys. Lett. **59**, 1272 (1991).
[12] O. Schulz, M. Strassburg, T. Rissom, S. Rodt, L. Reissmann, U. Pohl, D. Bimberg, M. Klude, D. Hommel, S. Itoh, K. Nakano, and A. Ishibashi, Phys. Status Solidi B **229**, 943 (2002).
[13] S.-H. Wei and A. Zunger, Appl. Phys. Lett. **72**, 2011 (1998).
[14] M. N. Huda, Y. Yan, S.-H. Wei, and M. M. Al-Jassim, Phys. Rev. B **78**, 195204 (2008).
[15] J. W. Liu, A. Kobayashi, S. Toyoda, H. Kamada, A. Kikuchi, J. Ohta, H. Fujioka, H. Kumigashira, and M. Oshima, Phys. Status Solidi B **248**, 956 (2011).
[16] J. Pezold and P. D. Bristowe, J. Mater. Sci. **40**, 3051 (2005).
[17] S.-K. Hong, T. Hanada, H. Makino, Y. Chen, H.-J. Ko, T. Yao, A. Tanaka, H. Sasaki, and S. Sato, Appl. Phys. Lett. **78**, 3349 (2001).
[18] A. Stroppa and M. Peressi, Phys. Rev. B **72**, 245304 (2005).
[19] A. Colli, E. Carlino, E. Pelucchi, V. Grillo, and A. Franciosi, J. Appl. Phys. **96**, 2592 (2004).
[20] A. Kley and J. Neugebauer, Phys. Rev. B **50**, 8616 (1994).
[21] H. H. Farrell and R. A. LaViolette, J. Vac. Sci. Technol. B **22**, 2250 (2004).
[22] H. H. Farrell and R. A. LaViolette, J. Vac. Sci. Technol. B **23**, 406 (2005).
[23] W. Kohn and L. J. Sham, Phys. Rev. **140**, A1133 (1965).
[24] P. Hohenberg and W. Kohn, Phys. Rev. **136**, B864 (1964).
[25] J. P. Perdew, K. Burke, and M. Ernzerhof, Phys. Rev. Lett. **77**, 3865 (1996).
[26] G. Kresse and J. Hafner, Phys. Rev. B **47**, 558 (1993).
[27] G. Kresse and J. Hafner, Phys. Rev. B **48**, 13115 (1993).
[28] G. Kresse and J. Furthmuller, Comput. Mater. Sci. **6**, 15 (1996).
[29] G. Kresse and D. Joubert, Phys. Rev. B **59**, 1758 (1999).

[30] H. J. Monkhorst and J. D. Pack, Phys. Rev. B **13**, 5188 (1976).
[31] J. P. Perdew and M. Levy, Phys. Rev. Lett. **51**, 1884 (1983).
[32] F. C. von der Lage and H. A. Bethe, Phys. Rev. **71**, 612 (1947).
[33] Y.-H. Li, X. G. Gong, and S.-H. Wei, Appl. Phys. Lett. **88**, 042104 (2006).
[34] S. P. Kowalczyk, J. T. Cheung, E. A. Kraut, and R. W. Grant, Phys. Rev. Lett. **56**, 1605 (1986).
[35] Y.-H. Li, A. Walsh, S. Chen, W.-J. Yin, J.-H. Yang, J. Li, J. L. F. Da Silva, X. G. Gong, and S.-H. Wei, Appl. Phys. Lett. **94**, 212109 (2009).
[36] W. G. Wilke and K. Horn, J. Vac. Sci. Technol. B **6**, 1211 (1988).
[37] R. S. Bauer and G. Margaritondo, Phys. Today **40**, 26 (2008).
[38] L. Vanzetti, X. Yu, A. Raisanen, L. Sorba, G. Haugstad, G. Bratina, and A. Franciosi, J. Cryst. Growth **117**, 573 (1992).
[39] S. P. Kowalczyk, E. A. Kraut, J. R. Waldrop, and R. W. Grant, J. Vac. Sci. Technol. **21**, 482 (1982).
[40] S.-H. Wei and A. Zunger, Phys. Rev. B **60**, 5404 (1999).
[41] J. Heyd, G. E. Scuseria, and M. Ernzerhof, J. Chem. Phys. **118**, 8207 (2003).
[42] L. Hedin, Phys. Rev. **139**, A796 (1965).
[43] A. Grüneis, G. Kresse, Y. Hinuma, and F. Oba, Phys. Rev. Lett. **112**, 096401 (2014).
[44] K. Steiner, W. Chen, and A. Pasquarello, Phys. Rev. B **89**, 205309 (2014).